PROCEEDINGS OF ISAP '96, CHIBA, JAPAN

INTERFEROMETRIC TECHNIQUE FOR DETERMINING THE AVERAGE HEIGHT PROFILE OF ROUGH SURFACES

Akira Ishimaru, Charles T. C. Le, Yasuo Kuga, Ji-Hae Yea, Kyung Pak, and Tsz-King Chan

Department of Electrical Engineering, University of Washington
Box 352500, Seattle, WA 98195-2500
Tel: (206)543-2169; Fax: (206)543-3842; E-mail: ishimaru@ee.washington.edu

Abstract

A new angular correlation phenomenon called the "angular memory effect" (AME) is applied to interferometric SAR (InSAR). Two transmitters illuminate the surface and the scattered waves are observed at two receivers. The mutual coherence function (MCF) for the scattered waves shows that the phase is linearly related to the average topographic height. This is extended to the two-frequency MCF which shows the relationship between the pulse arrival times and the height profile. The theoretical results are confirmed by experiments and numerical simulations.

1 Introduction

In recent years, interferometric technique has been applied to Synthetic Aperture Radar (InSAR) for obtaining global topographic maps and other geophysical applications, and extensive theoretical and experimental studies have been reported [1, 2]. Recently, we have been involved in the study of the angular correlation of scattered waves from rough surfaces and have made detailed studies of the "memory effects" [3]. In this paper, we extend our previous study of the memory effect to include the slowly varying average height variations and the relationship with InSAR. Two transmitters at different angles θ_i and θ_i' illuminate the surface and the MCF for the corresponding scattered waves at two different angles θ_s and θ_s' are calculated (Fig. 1). The theory is based on the Kirchhoff approximation applicable to rough surfaces with large radii of curvature [3]. It is shown that the phase of the MCF is related to the average surface profile, and therefore, the height profile can be determined by the measurement of the correlation of the scattered waves. The MCF is expressed in the memory diagram which shows the correlation as a function of the second incident θ_i' and scattered θ_s' for given reference incident θ_i and scattered θ_s. This gives the general characteristics of the amplitude and the phase of the MCF, and clearly shows the effects of the locations of the antennas on the sensitivity of the correlation. Next we extend the theory to the two-frequency MCF and the time-domain response. It shows the relationship between the pulse arrival time and the surface height profile. Millimeter wave experiments and Monte-Carlo simulations are conducted and the results are compared with the theory.

2 The Mutual Coherence Function

Using the first-order Kirchhoff approximation and the stationary phase approximation, we express the mutual coherence function between waves observed at the scattered angles θ_s, θ_s' due to

waves incident at θ_i, θ_i' as

$$< \psi(\bar{K})\psi^*(\bar{K}') = FF'^* G_o G_o'^* < II'^* > \tag{1}$$

where $F = -i[|\bar{K} - \bar{K}_i|^2/(K_z - K_{iz})]r$; $F' = -i[|\bar{K}' - \bar{K}_i'|^2/(K_z' - K_{iz}')]r'$; G_o and G_o' are the free-space Green's functions; and $< II'^* >= \int d\bar{x} \int d\bar{x}' \exp(-i\bar{v}\cdot\bar{x} - iv_z f - i\bar{v}'\cdot\bar{x}' - iv_z' f')$; $\bar{K}, \bar{K}_i$ are the propagation vectors; r is the reflection coefficient; the coordinates of the target are represented by $(\bar{x}, f(\bar{x}))$ where f denotes the height above a flat reference plane; $\bar{v} = (\bar{K} - \bar{K}_i)_{xy}$, $v_z = (\bar{K} - \bar{K}_i)_z$; and the prime represents the corresponding variables for the second beams.

The surface height f is decomposed into two parts $f =< f_c > + f_r$, where $< f_c >$ denotes the slowly varying component representing the average topography height with slope $\bar{m} = \frac{\partial < f >}{\partial x}\hat{x} + \frac{\partial < f >}{\partial y}\hat{y}$, and f_r is the small fluctuating component having a Gaussian distribution with rms height σ and a Gaussian correlation function $C(x_d) = \exp(-x_d^2/l^2)$ where l is the correlation length. For the antenna patterns, we use Gaussian beam waves $|W|^2 = \exp(-x^2/L^2)$ with L being the illumination area . Following the approach used in [3], we were able to obtain a closed form solution.

$$< II'^* >= F_1 F_2 \tag{2}$$

$$F_1 = (\frac{\pi l^2}{\nu_z \nu_z' \sigma^2}) \exp[-\frac{1}{2}(\nu_z - \nu_z')^2\sigma^2] \exp[-\frac{|\nu_c + \bar{m}\nu_{zc}|^2 l^2}{4\nu_z\nu_z'\sigma^2}] \tag{3}$$

$$F_2 = (\pi L^2) \exp[-\frac{\nu_d^2 L^2}{4}] \exp[-i\nu_{zd} < f_c >] \tag{4}$$

where $D(x_d) = 2 < f_r^2 > (1 - C(x_d))$; $\bar{x}_c = (1/2)(\bar{x} + \bar{x}')$, $\bar{x}_d = (\bar{x} - \bar{x}')$, $\bar{v}_c = (1/2)(\bar{v} + \bar{v}')$, $\bar{v}_d = \bar{v} - \bar{v}'$, $v_{zc} = (1/2)(v_z + v_z')$, and $v_{zd} = v_z - v_z'$.

The effects of the average topographic height are now visible. The degree of correlation depends on its slope $\bar{m}$ in Eq. (3). The average height $< f_c >$ produces a phase shift $\phi = \nu_{zd} < f_c >$ in Eq. (4).

3 The Two-Frequency MCF

The MCF is applicable for continuous wave (CW). For pulse problems such as InSAR, we need the two-frequency MCF [4], which is the correlation (in the frequency domain) of two waves (already at different angles) at different frequencies. The Fourier transform of the two-frequency MCF then gives the ACF in the time domain. The correlation of the two scattered waves $E_s(t_1)$ and $E_s'(t_2)$ at two different times t_1 and t_2 can be written as [4]

$$< E_s(t_1)E_s'(t_2) >= \int\int d\omega_1 d\omega_2 U_i(\omega_1)U_i^*(\omega_2)\Gamma \exp(-i\omega_1 t_1 + i\omega_2 t_2) \tag{5}$$

where Γ is the two-frequency MCF given in the previous section; $U_i(\omega) = \int u_i(t)\exp(i\omega t)$ is the spectrum of the transmitted pulse $u_i(t)$ assumed to have a Gaussian profile $u_i(t) = A_o \exp(-i\omega_o t)\exp(-t^2/T_o^2)$. We now study the effects of the pulse arrival times on the interferometric phase $\phi = \nu_{zd} < f_c >$. Thus the two-frequency MCF is written as (ignoring other factors)

$$\Gamma = e^{-i\nu_{zd} < f_c >} e^{ik(R_1 + R_2) - ik'(R_1' + R_2')} \tag{6}$$

where R_1 and R_2 are the distances from the reference transmitter and receiver to the flat surface, and similarly for the primed variables. Eq. (5) can now be evaluated and the result is (ignoring

other unimportant factors)

$$< E_s(t_1)E_s'(t_2) > \propto \exp[-(\gamma_c < f_c > /c + t_c - R_c/c)^2] \exp[-i\omega_o(\gamma_d < f_c > /c + t_d - R_d/c)] \exp[-(\gamma_d < f_c > /c + t_d - R_d/c)^2/(2T_o^2)] \quad (7)$$

where $\gamma_d = (\cos\theta + \cos\theta_i) - (\cos\theta' + \cos\theta_i')$, $\gamma_c = (1/2)[(\cos\theta + \cos\theta_i) + (\cos\theta' + \cos\theta_i')]$, $t_d = t_1 - t_2$, $t_c = (1/2)(t_1 + t_2)$, $R_d = (R_1 + R_2) - (R_1' + R_2')$, and $R_c = (1/2)[(R_1 + R_2) - (R_1' + R_2')]$.

The second exponential term gives the total phase shift due to different observing angles ($\omega_o\gamma_d < f_c > /c$), different observing times ($\omega_o t_d$), and different ranges ($\omega_o R_d/c$). The third exponential term yields a small decrease in the correlation, in addition to the decorrelation in the previous section. The first exponential term provides the arrival time of the pulses (the peak of the exponential), which is on average R_c/c (average propagation path), minus $\gamma_c < f_c > /c$ (earlier time due to the average topographic height).

4 The Millimeter-Wave Experiment and Monte-Carlo Simulation

To validate the predicted phase from the theory, we performed millimeter-wave scattering experiments (MMWE) at $\lambda = 3$ mm ($f = 100$ GHz). The experimental setups and procedures are well documented in [5]. The antennas were scanned along the memory line for high level of correlation [3], which implies higher accuracy in the phase measurement. For given reference and scanning angles, we raised the test surface in the vertical direction from zero to 17λ (5 cm). This simulates the average topography height. We also carried out Monte-Carlo simulation using the banded matrix iterative approach/canonical grid (BMIA/CAG) method [6]. Rough surfaces of different characteristics were used to study their effects on the interferometric phases, and to demonstrate the robustness of using the AME technique to get the phase of InSAR. Comparison between numerical and theoretical results at normal reference incident angles is shown in figure 2 for $(\sigma, l) = (0.25\lambda, 0.6\lambda)$ and $\theta_i' = 2.5^o$ and 5^o. For the MMWE, we chose a rough surface with $(\sigma, l) = (0.25\lambda, 0.25\lambda)$ and measured the phase. Comparisons between theoretical, numerical and experimental results are shown in figure 3. The uncertainty in the measured phase is also shown as error bars.

5 Conclusion

We have shown that the AME can be applied to InSAR for the retrieval of topographic height. The interferometric phase is *not* sensitive to the surface roughness, thus showing the robustness of the technique. Validation of the theory by performing MMWE and numerical simulation yields good agreement.

References

[1] S.N. Madsen, H.A. Zebker, and J. Martin, "Topographic mapping using radar interferometry: processing techniques", *IEEE Trans. Geosci. Rem. Sens.*, **31**, 246-256, (1993)

[2] E. Rodriguez and J. Martin, "Theory and design of interferometric synthetic aperture radars", *IEE Proceedings*, **139**, 147-159, (1992)

[3] C. Le, Y. Kuga, and A. Ishimaru, "Angular correlation function based on the second-order Kirchhoff approximation and comparison with experiments", *J. Opt. Soc. Am. A*, accepted for publication, (1996).

[4] A. Ishimaru, *Wave Propagation and Scattering in Random Media.* New York: Academic, (1978), pp. 96.

[5] T-K Chan, Y. Kuga, and A. Ishimaru, "Angular memory effect of millimeter-wave scattering from two-dimensional conducting random rough surfaces", *Radio Science*, accepted for publication, (1996).

[6] L. Tsang, C.H. Chan, K. Pak, and H. Sangani, "Monte-Carlo simulations of large-scale problems of random rough surface scattering and applications to grazing incidence with the BMIA/canonical grid method", *IEEE Trans. Antenn. Propa.*, 43, 851-859, (1995).

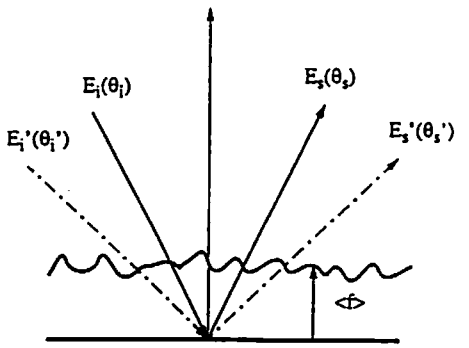

Figure 1: The scattering geometry.

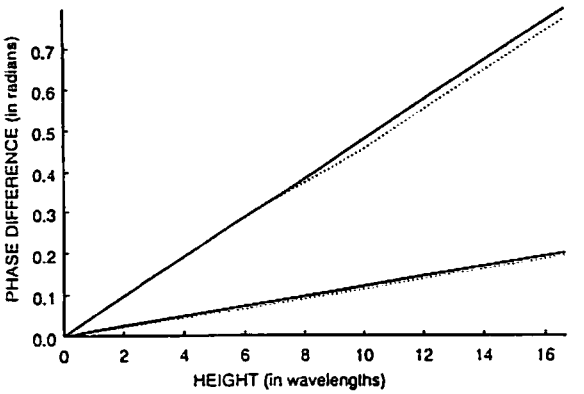

Figure 2: Interferometric phases: theoretical (solid), numerical (dotted). Reference angles $(\theta_i, \theta_s) = (0°, 0°)$. Upper curves $(\theta_i' = 5°)$, lower curves $(\theta_i' = 2.5°)$.

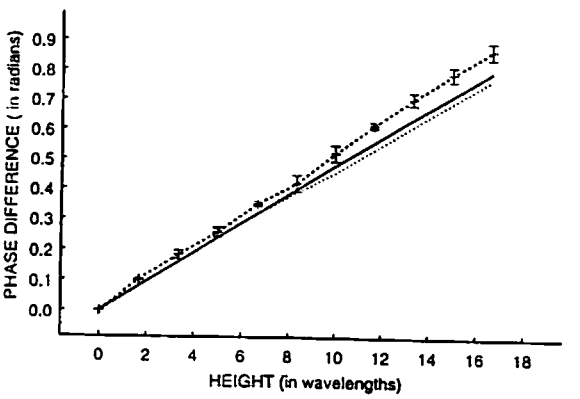

Figure 3: Interferometric phases: theoretical (solid), numerical (dotted), experimental (dashed). Reference angles $(\theta_i, \theta_s) = (0°, 0°)$; $\theta_i' = 5°$.